Thermal-light heterodyne spectroscopy with frequency comb calibration

CONNOR FREDRICK[1,2,*], FREJA OLSEN[3], RYAN TERRIEN[3], SUVRATH MAHADEVAN[4,5], FRANKLYN QUINLAN[2], AND SCOTT A. DIDDAMS[1,2,†]

[1] Department of Physics, University of Colorado Boulder, 440 UCB Boulder, CO 80309, USA
[2] Time and Frequency Division, National Institute of Standards and Technology, 325 Broadway, Boulder, CO 80305, USA
[3] Carleton College, One North College Street, Northfield, MN 55057, USA
[4] Department of Astronomy & Astrophysics, 525 Davey Laboratory, The Pennsylvania State University, University Park, PA 16802, USA
[5] Center for Exoplanets and Habitable Worlds, 525 Davey Laboratory, The Pennsylvania State University, University Park, PA 16802, USA
[*] connor.fredrick@colorado.edu
[†] scott.diddams@nist.gov

Compiled August 12, 2021

Precision laser spectroscopy is key to many developments in atomic and molecular physics and the advancement of related technologies such as atomic clocks and sensors. However, in important spectroscopic scenarios, such as astronomy and remote sensing, the light is of thermal origin and interferometric or diffractive spectrometers typically replace laser spectroscopy. In this work, we employ laser-based heterodyne radiometry to measure incoherent light sources in the near-infrared and introduce techniques for absolute frequency calibration with a laser frequency comb. Measuring the solar continuum, we obtain a signal to noise ratio that matches the prediction given by the thermal photon distribution and our system's quantum efficiency. With absolute frequency calibration we determine the center frequency of an iron line in the solar spectrum to MHz-level uncertainty in under 10 minutes, a fractional precision 1/4000 the linewidth. Additionally, we propose concepts that take advantage of refractive beam shaping to decrease pointing instabilities by nearly 100x, and of frequency comb multiplexing to increase data acquisition rates and spectral bandwidths by comparable factors. Taken together, our work brings the power of telecommunications photonics and the precision of frequency comb metrology to laser heterodyne radiometry, with implications for solar and astronomical spectroscopy, remote sensing, and precise Doppler velocimetry.

http://dx.doi.org/10.1364/ao.XX.XXXXXX

1. INTRODUCTION

Optical frequencies are the most precisely measured physical quantities. The best laser spectroscopy has fractional uncertainty at the level of 1×10^{-18} [1, 2], and optical frequency combs [3] have the capability to coherently synthesize and compare ratios of optical frequencies with uncertainty in the range of 10^{-21} [4–6]. However, for many important optical and infrared systems of spectroscopic interest—such as those in astronomy and atmospheric remote sensing—the light to be analyzed does not come from a laser, but is thermal in origin. Here, one typically resorts to interferometric (Fourier transform) or diffractive (grating) spectrometers for spectral analysis. In such spectrometers, wavefront errors, instrument instabilities, and technical constraints on size limit the achievable precision as well as practicality. In this regard, heterodyne spectroscopy [7] between a laser and a thermal source remains a compelling option for making spectral measurements at known frequencies instead of at inferred wavelengths. Commonly called laser heterodyne radiometry (LHR), such thermal heterodyne has it roots in radio-astronomy [8, 9] and has generally only been implemented for astronomy [10–13], trace-gas sensing, and atmospheric spectroscopy [14–16] in the infrared region (e.g. 10 µm). However, with the ubiquity of high quality telecom fiber optic components there is growing interest in the use of LHR in the near-infrared region of the spectrum (1.5-1.7 µm), for remote detection and spectroscopy of gases in the earth's atmosphere [17–21].

Figure 1 illustrates the operational concepts and parameters of our LHR system (see the Supplement for a detailed description of the experimental setup). Here, the source of interest is the Sun, but in general it can be any object that emits or reflects incoherent radiation. Through subsequent absorption and emission processes, either from atomic and molecular species in the Sun's own photosphere or from earth's atmosphere, spectroscopic information becomes imprinted on the thermal spectrum. A nar-

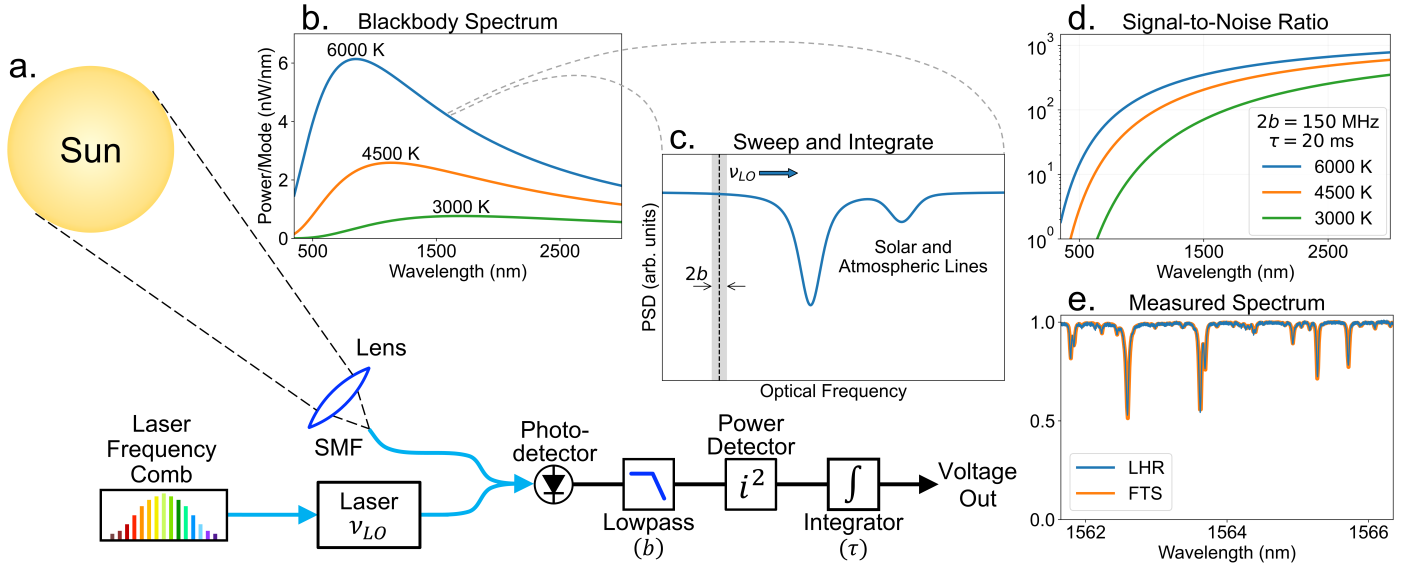

Fig. 1. Laser heterodyne radiometry (LHR) concepts. **(a)** Light from a thermal source, such as the Sun, is coupled into a single-mode optical fiber (SMF) where it is heterodyned with a laser and then processed with a few simple radio frequency (RF) components. **(b)** The single-mode power spectral density (PSD) of a thermal source at various blackbody temperatures (solar surface is ∼5800 K). **(c)** The local oscillator (LO) converts the spectral information from a small region about frequency ν_{LO} to the RF baseband. This information is sent through a low-pass filter (bandwidth b), power detector, and integrator (averaging time τ) to provide a signal proportional to the power within the optical bandwidth $\Delta\nu = 2b$. The full spectral profile can be reconstructed by scanning ν_{LO}. **(d)** The theoretical signal-to-noise ratio for effective bandwidth $2b = 150$ MHz and averaging time $\tau = 20$ ms. **(e)** The solar spectrum recorded near 1564 nm using LHR and with a Fourier-transform spectrometer (FTS) [22, 23].

row linewidth local oscillator laser (LO) is heterodyned with the thermal light and spectral information at difference frequencies with respect to the LO are mixed down into the radio frequency (RF) domain. The RF power within an electrical bandwidth b is proportional to the optical power in optical bandwidth $\Delta\nu = 2b$ centered on the LO frequency. This bandwidth sets the spectral resolution and can range from Hz to GHz using common radio-frequency electronics, which is a significant advantage of LHR. Without the complexity of large free-space delays or diffractive elements, LHR can achieve high spectral resolution in a very compact apparatus. Scanning the LO frequency and recording the down-converted RF power reconstructs the optical spectrum.

In all such LHR measurements, the stability of the LO frequency ultimately determines the spectral accuracy, and passive etalons, molecular absorption cells, or wavelength meters have been used to track the relative frequency of the LO. However, these frequency references are not tied to fundamental frequency standards, and may drift on their own or have unknown absolute accuracy. In this paper, we introduce laser frequency comb (LFC) technology to LHR, thereby providing absolute frequency traceability at the kilohertz level and the capability of averaging over indefinite timescales. Our system achieves spectral resolving power of R=$\nu/\Delta\nu$=1,000,000 and is built on robust fiber-integrated lasers in the 1.5 µm region. Utilizing fiber-integrated laser power control and balanced photodetection, we largely remove technical noise and achieve sensitivity within 1 dB of the fundamental shot-noise limit (see Supplement).

We illustrate the advantages of this approach with LHR spectroscopy of laboratory, solar, and atmospheric sources. In studies of a solar iron line, we measure a signal-to-noise ratio (SNR) of about 300 in 20 ms and with 200 MHz resolution bandwidth, a number which exactly agrees with the theoretical prediction. The full spectrum of the line is swept out in 10 s, and after averaging 60 spectra we are able to determine the line center to a precision of about 1 MHz, splitting the 3.7 GHz linewidth by a factor of 2.5×10^{-4}. Similar fractional precision is obtained on the HCN P28 line with a laboratory gas cell, although the narrower linewidth leads to an uncertainty of only 200 kHz in the determination of the center frequency. These numbers are limited by the SNR of our experiment, the intrinsic frequency uncertainty is still orders of magnitude lower and is ultimately only limited by the atomic frequency reference used to stabilize the frequency comb.

The potential for absolute frequency calibration and improved long-term stability makes our approach relevant to a large body of work in atmospheric trace gas spectroscopy and solar astrophysics. In the latter field, precise knowledge of spectral line shapes and frequency shifts can inform models of stellar magnetism and photospheric dynamics for efforts aimed at disentangling such activity from center-of-mass Doppler shifts [24, 25]. This technique also holds the potential to directly achieve cm/s level radial velocity precision (10-100 kHz) on the Sun, which has not been demonstrated to date. The ability to do so is a critical and open question in the astronomical community searching for terrestrial-mass exoplanets in the habitable zones of nearby stars [26]. Furthermore, we lay the groundwork for additional modalities of direct frequency comb spectroscopy of non-laser sources [27, 28]. This includes massively-parallel heterodyne with frequency combs that could be employed not only for spectroscopy but for long baseline phased-array imaging [29].

A. Theoretical background

The theory of LHR has been thoroughly covered by others [9, 30], and we simply state the important considerations for the system

described in this paper. A single optical mode can only couple to a single statistical-mechanical thermal mode. The antenna theorem limits the product of the effective aperture (A) and field of view (Ω) of an optical mode to the square of its wavelength (λ), $A\,\Omega = \lambda^2$ [31]. This can also be viewed as the power within the area at the receiver over which the thermal source light is spatially coherent and the source remains an unresolved point. The power coupled into a single mode is maximized when the field of view is completely filled by the thermal source:

$$P_{\max} = h\nu\,\langle n\rangle\,\Delta\nu \tag{1}$$

where $h\nu$ is the photon energy, $\Delta\nu$ is the optical bandwidth, and $\langle n\rangle$ is the mean photon occupancy given by the Planck or Bose-Einstein distribution, $\langle n\rangle = (\exp[h\nu/kT]-1)^{-1}$. This expression, converted to a spectral density in terms of wavelength, is shown in Fig. 1(b) for a few blackbody temperatures relevant to the Sun and other common stellar types. Note that at 1550 nm, there is only 5 pW within a resolution bandwidth of $\Delta\nu = 150$ MHz for a thermal source with the temperature of the Sun (roughly 4 nW/nm single-mode power spectral density). The shape and extent of the optical mode is important for how information is retrieved spatially (see Section 4), but as long as the thermal source is larger than the field of view, improved imaging or tighter focusing onto the fiber will not change the coupled power. For standard single-mode fiber (SMF) at 1550 nm, only a simple collimating lens with mm scale aperture is required to achieve a field of view smaller than the $\sim 0.5^\circ$ angular diameter of the Sun.

The heterodyne process is equivalent to passing the thermal light through a quantum-limited, phase-insensitive amplifier. If the LO shot noise dominates other sources of noise, this leads to the following signal-to-noise ratio [32]:

$$\mathrm{SNR} = \frac{\eta\,\langle n\rangle}{1+\eta\,\langle n\rangle}\sqrt{\Delta\nu\,\tau} \tag{2}$$

where τ is the averaging time and η is the probability that a photon emitted by the blackbody arrives at the detector and results in a photoelectron. The efficiency factor η includes all transmission losses as well as the detection quantum efficiency. The additional factor of $\eta\,\langle n\rangle$ in the denominator is due to thermal photon bunching and has important implications. No matter how many photons there are, or how hot the source is, the first term in Eq. 2 is always less than 1. This means that the main path towards useable signal-to-noise ratios is to increase the optical bandwidth or the averaging time. The bunching term is also why LHR has typically only been considered for the mid- and far-infrared, as starting with a relatively large number of photons gives an SNR that is both larger and less sensitive to optical loss. The signal-to-noise ratio rapidly drops off at short wavelengths due to reduced photon counts, but as seen in Fig. 1(d), the SNR can assume significant values in the near-infrared for the reasonable experimental parameters we employ.

2. SYSTEM CHARACTERIZATION

A. Laboratory Gas Cell

We conducted LHR experiments using an amplified spontaneous emission (ASE) source in the lab to explore systematics independent of instabilities due to telescope tracking, relative Solar velocity and rotation, as well as variable Solar flux (e.g. due to cloud cover). The broadband light from an unseeded semiconductor optical amplifier was attenuated to approximate the power spectral density of sunlight. Absorption lines imparted on the ASE by an HCN gas cell (NIST SRM 2519a [33]) served as stable spectral features to measure with the LHR setup. The results from a series of scans of the P28 transition spanning 36 hours are shown in Fig. 2. The scan range of this measurement was restricted to a 4 GHz region about the P28 transition. With an effective averaging time of 200 ms and resolution bandwidth of 200 MHz, each scan was collected in 6 s.

The amplitude and frequency noise of this measurement are analyzed by comparing the data against a template formed from a spectrally-aligned average of the entire dataset (see Supplement for details). The data from the spectrally-aligned traces are compared against the average in Fig. 2(a). Since the curves are normalized to the same mean amplitude and shifted to the same line center frequency, the residuals solely represent the relative amplitude noise. As expected from amplitude fluctuations due primarily to shot noise, the distribution of the noise is Gaussian. The effective line center shift of each trace is calculated by finding the frequency shift that maximizes the trace's cross-correlation with the template. As seen in Fig. 2(b), over the first few decades the frequency instability of the HCN line agrees with the white amplitude noise limit calculated from the line shape (described in Supplement). This indicates that amplitude fluctuations dominate the short and medium term frequency instability and the measurement is limited purely by the SNR.

The origin of the 200 kHz noise floor seen in the last decade is less certain. As discussed in the next section, the noise floor is not due to frequency comb calibration uncertainty. Temperature shifts are largely ruled out when we use the temperature sensitivity of the lines given in [34] with our measured lab temperature shifts. In addition, we also did not find a significant coupling between frequency shifts and variations of the mean LHR amplitude. While unexplored, there could be a polarization induced effect due to the HCN system being connectorized using non-polarization maintaining fibers. This is an area that needs further study, but regardless of the true source or cause of the noise floor it does not yet represent a concern for the solar measurements we performed. With the current setup the obtainable averaging times on the Sun are less than 1000 s, which is still within the $1/\sqrt{\tau}$ averaging region of the HCN dataset.

B. Absolute Frequency Calibration

A major benefit of the laser frequency comb is that it allows for absolute frequency calibration. The frequency of the LO is tracked by heterodyning it against a laser frequency comb (see Fig. 1 and Supplement). As the LO laser is continuously swept in time, the spectrum of the frequency comb is mapped out using the same LHR techniques as for the thermal light. The LFC provides a reference grid traceable to the SI second, with instability of a few parts in 10^{-13} or better on timescales from seconds to years ($\sim$20 Hz frequency precision at 1550 nm). This precise reference has been absent from other LHR measurements, and we believe it will be key to the long-term averaging and day-to-day repeatability required to meaningfully track the center frequency and line shape of solar or atmospheric lines. Details of the calibration are provided in earlier work [35] and the Supplement.

To estimate an upper limit on the sweep-to-sweep calibration uncertainty we injected LFC light into both arms of the LHR system. The frequency calibration procedure was applied using data from the first arm while cross-correlation was used on data from the second to determine the trace-to-trace frequency shift. For 5 s traces spanning a 15 GHz optical window, this comb

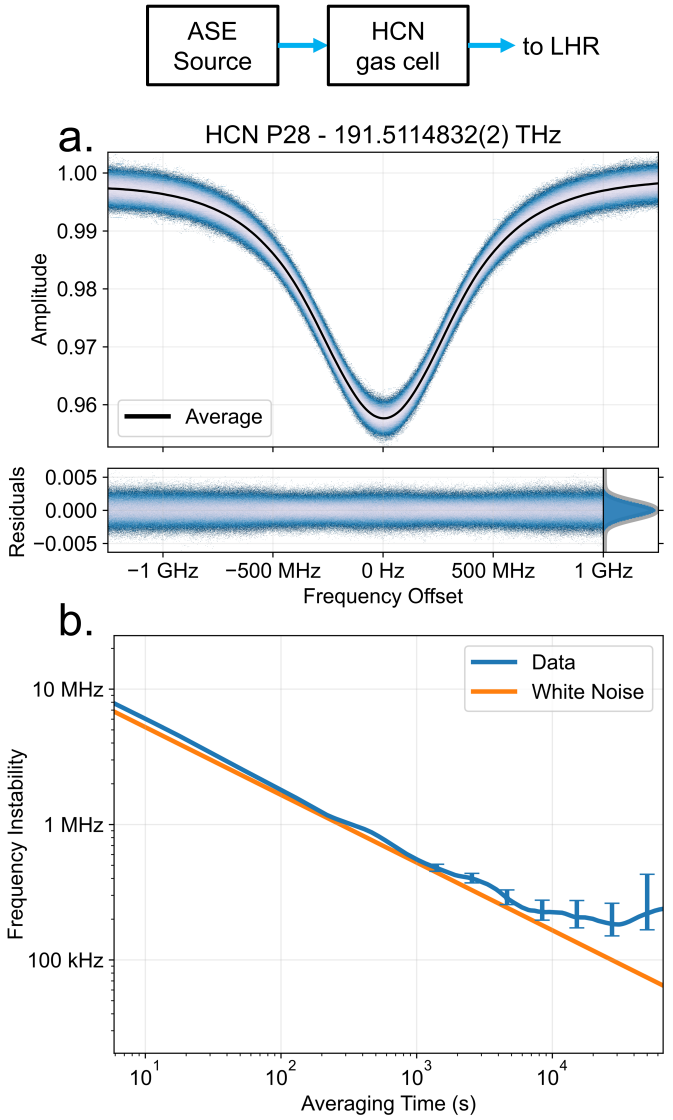

Fig. 2. An $H^{13}C^{14}N$ reference cell [33] is illuminated by amplified spontaneous emission (ASE). **(a)** LHR of the P28 line of HCN near 1565.40 nm [34]. The data represents all 22,281, 6 s traces taken over the course of 36 hours. The amplitude has been normalized to the background continuum and the color is scaled to the density of points given by the two-dimensional histogram of the entire dataset. The residuals with respect to the average are plotted below. The inset at the bottom right shows the histogram of the residuals outlined by a Gaussian distribution of the same width in grey. **(b)** The Allan deviation of the retrieved line centers and the theoretical white amplitude noise limit. See text and Supplement for details.

versus comb measurement yielded a frequency uncertainty at the few 10's of kHz level, approaching the 1 kHz level after 1000 s of averaging.

Due to additional RF processing, the absolute frequency of our LHR system is given by a modified comb equation:

$$\nu = f_c + f_0 + \frac{f_R}{4}\left(n + \frac{1}{2}\right) - f_{dly} \quad (3)$$

where f_c is the line center frequency relative to the calibration tick given by integer index n, f_0 and f_R are the carrier-envelope offset frequency and repetition rate of the frequency comb, and f_{dly} is the effective frequency axis shift due to the time delay between the two arms (see Supplement). The line center frequency (f_c) is the sum of the template's center frequency, found through fitting a Voigt profile to the template, and the average frequency shift of the individual traces from the template. Calibration precision is improved through electronic mixing which reduces the effective f_R and increases the number of calibration ticks by a factor of 4 [35]. The delay frequency shift (f_{dly}) is calculated from the scan rate of the LO laser and the time delay of the averaging low-pass filters, which were measured to effective frequency precisions 5 to 10 times better than the minimum given by the Allan deviations of both the HCN and solar measurements.

An estimate of the HCN line's absolute frequency is used to determine the absolute comb line number (n). Since the SRM 2519a HCN reference cell is only certified for P-branch frequencies up to the P27 transition [33], it does not report a frequency specification for the P28 transition. We estimate our cell's P28 frequency by adding the pressure shifts extrapolated from the last few certified lines to the vacuum line center calculated in reference [34]. That estimate was found to be within ∼2 MHz of the frequency given by our LHR measurement and an integer comb number, which results in a final absolute frequency of 191.5114832(2) THz for the P28 transition of our gas cell. For comparison, a 2 MHz error is well within the ∼10 MHz $\pm 1\sigma$ certified uncertainty for the nearest line at P27.

3. RESULTS ON THE SUN

Using this system we observed a neutral iron line (Fe I) in the solar spectrum with a vacuum wavelength near 1565.279 nm [36, 37]. Fig. 3 illustrates the spectral profile and amplitude noise from the unobstructed (cloud free) traces of an observing run that extended one hour. Each trace, spanning 27.5 GHz, was taken over a 10 s period and was processed using the same procedures as described in the previous section and in the Supplement for the measurement of the HCN line. While the full shape of the iron line only spans about 15 GHz, the additional scan range facilitated calculation of the absolute frequency by extending over the positions of both the iron and P28 HCN lines using a single sweep configuration. After the solar measurements finished, the input to the LHR arm was switched to the ASE illuminated HCN gas cell and its known line center was used to determine the reference comb line number for absolute frequency calibration of the solar data.

It is interesting to examine the solar data's signal-to-noise ratio as compared to the theoretical value for a thermal source. For this purpose, we take the standard deviation of the residuals roughly 15 GHz away from the line center over a 4 GHz window where the measured signal was closest to the background continuum level. With the continuum normalized to 1, the reciprocal of that standard deviation defines the data driven SNR. The predicted SNR is calculated using equation 2. The total quantum efficiency is 0.77, which accounts for the detector's quantum efficiency (0.82) and the transmission through the fiber connectors and splitter (0.93). The effective temperature within the field of view of the Gaussian mode is estimated to be 6000 K ($\langle n \rangle \approx 0.27$), given the nominal solar disk temperature of 5800 K [38] and the limb darkening profile at 1565 nm as measured in reference [39] (the center of the solar disk is brighter than the average due to limb darkening and so has a larger effective temperature). Using the above values, and the system's effective averaging time of 21 ms and noise bandwidth of 150 MHz, the predicted SNR is

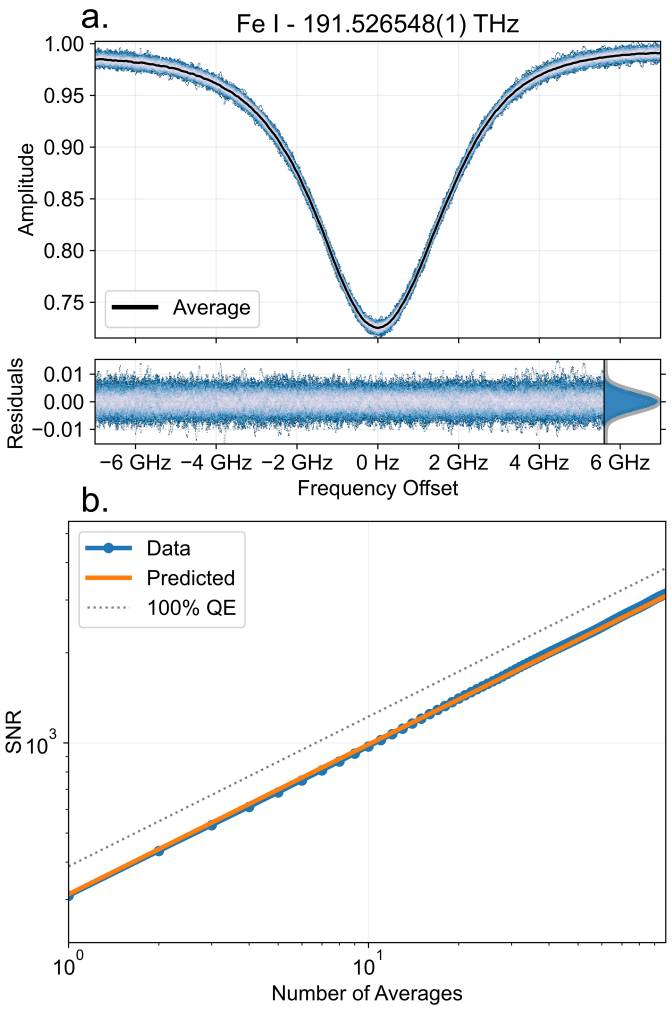

Fig. 3. LHR measurement of a neutral iron line in the solar spectrum. The absolute frequency is given in the frame of the solar system barycenter. **(a)** Fe I line near 1565.279 nm [36, 37]. The data represents 196, 10 s traces taken over the course of 1 hour. These traces were selected for high SNR which became degraded due to intermittent clouds. The amplitude has been normalized to the background continuum and the color is scaled to the density of points given by the two-dimensional histogram of the entire dataset. Each trace has been frequency shifted to a common center and the resulting average is shown as the black line. The residuals with respect to the average are plotted below. The inset at the bottom right shows the histogram of the residuals outlined by a Gaussian distribution of the same width in grey. **(b)** The measured and theoretical SNR of the background continuum with respect to the residuals. Using equation 2, the predicted single trace SNR is 313. The data gives an SNR of 309 and follows $\sqrt{N}$ averaging up to an SNR of over 3000 within 100 averages. The grey dotted line, which starts at an SNR of 390, represents the predicted SNR assuming the same setup but with no loss and perfect detection efficiency.

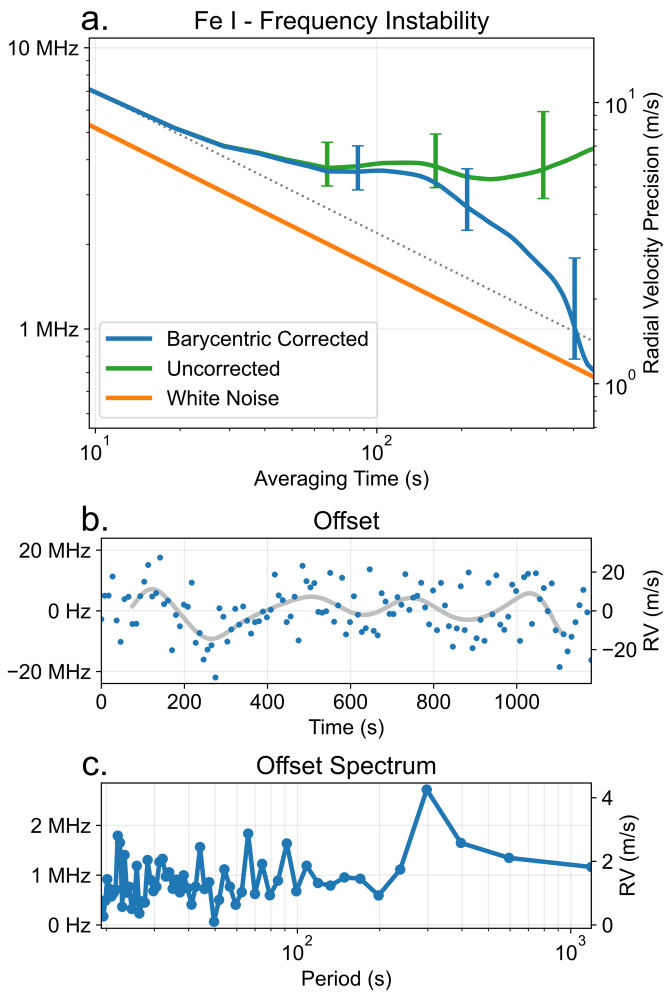

Fig. 4. Frequency stability analysis of the iron line in Fig. 3. The data represents the first 125 traces of the observation, which is cut off early due to clouds and drifting alignment of the solar tracker. **(a)** The Allan deviation of the retrieved line centers and the theoretical white amplitude noise limit. The green line is the instability as measured in the lab and the blue line is the calculated instability in the reference frame of the solar system barycenter. Both have an initial value of 7.1 MHz per 10 s trace. The error bars represent the $\pm 1\sigma$ confidence intervals, while the grey dotted line represents $1/\sqrt{\tau}$ averaging and is included to help guide the eye. The orange line is the white amplitude noise limit, calculated from the line shape, and starts at 5.3 MHz. **(b)** The frequency offset of the barycentric corrected data in the time domain. After only a few points the frequency instability is dominated by a low frequency perturbation that occurs at the roughly 5 minute time scale characteristic of solar surface oscillations. The grey line, calculated through a weighted local polynomial filter, reveals those fluctuations to the eye. **(c)** The spectral amplitudes of the data in part (b), again demonstrating a prominent peak at about 5 minutes.

313. The SNR calculated purely from the data is 309, which demonstrates remarkable agreement with the fundamental detection limits dictated by Eq. 2. Additionally, the data shows the SNR improving with $\sqrt{N}$ averages, consistent with white noise, reaching a value of 3150 at 98 averages.

The central frequency of the line was tracked using the same cross-correlation procedure as described above and in the Supplement. The Allan deviation is shown in Fig. 4(a). The extracted line center instability of 7.1 MHz per 10 s trace is slightly higher

than predicted for purely white amplitude noise, but still represents a measurement precision of 1 part in 520 relative to the 3.7 GHz line width. However, because of the Doppler shift due to the relative motion between the Sun and the LHR system on the surface of the Earth, that value does not significantly improve after 10 minutes of averaging. Barycentric correction, using the algorithms from references [40, 41], removes that effect and calculates the expected frequency as seen by an observer far outside the solar system and at rest with respect to the solar systems' center of mass. Applying that correction, the instability averages down and is potentially reduced to below 1 MHz after 10 minutes, a precision which splits the line to better than 1 part in 4000. Examining the time domain frequency offsets in Fig. 4(b-c), the short term stability appears to be limited by the p-mode surface oscillations of the Sun, which have characteristic periods around 5 minutes. At timescales longer than shown here, the instability of the solar tracker becomes significant and the precision degrades due to pointing errors asymmetrically coupling the field of view into the Sun's large rotational Doppler shift. Below we present a photonic solution to this issue.

4. DISCUSSION AND FUTURE WORK

These experiments illustrate the present capabilities of our frequency-comb-calibrated LHR setup for precision spectroscopy, but several important opportunities and open questions remain about the full potential of this approach. The most immediate is the extension of the solar measurements to longer averaging times. Spectral information from across the Sun's surface is weighted by the antenna pattern given by the distribution of the optical mode in the far-field [31]. The present results were obtained with optics that coupled light into the SMF from only ∼25% of the solar disk. This leads to solar tracking errors manifesting as spectroscopic noise, as light from the eastern and western limbs of the solar disk have oppositely signed Doppler shifts due to the Sun's rotational motion. There are two options to minimize this effect, reduce the solar tracking errors and/or manipulate the antenna pattern to reduce the sensitivity to misalignment. The first could be accomplished through active feedback that locks to the bright center of the solar disk, while an attractive solution for the second is to employ a flat-top beam shaper. In contrast to those based on diffusers, which have been applied to great effect in precision astronomical photometry [42], the beam shapers proposed for use with LHR are single-mode in nature. Such beam shapers are common in laser machining and use refractive or diffractive elements to convert a single-mode Gaussian profile in the near-field into a flat-top profile in the far-field without introducing a speckle pattern. Fig. 5 compares the efficiency and pointing sensitivity of two Gaussian distributions with a flat-top profile provided by the manufacturer Holo/Or. While only a small perturbation for these beam shapes, the pointing sensitivity calculation included models for limb darkening [39] and the latitude variability of the Sun's rotational velocity [43]. In comparison to a Gaussian mode profile, a well matched top-hat aperture reduces the tracking sensitivity by 100×. A flat-top shape would uniformly integrate information from the entire solar disk, viewing the Sun as if it were an unresolved star. This would have the additional benefit of allowing such LHR observations to be directly compared to measurements made by more traditional multi-mode instruments, which do not have restrictive antenna patterns, allowing the lessons learned studying the Sun to be more easily transferred to the study of distant stars.

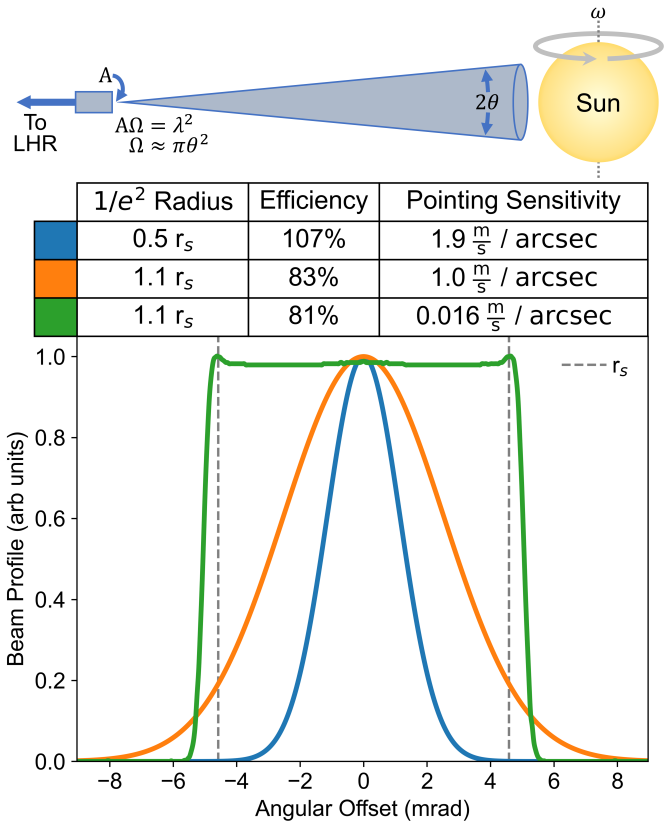

Fig. 5. Heterodyne Antenna Pattern and Pointing Sensitivity. *(blue)* Gaussian mode with radius 0.5 times the solar radius (r_s), *(orange)* Gaussian mode with radius $1.1r_s$, *(green)* flat-top mode with radius $1.1r_s$. The efficiency is normalized to the brightness given by the nominal solar temperature [38] and includes the effects of limb darkening [39]. The pointing sensitivity is the theoretical Doppler shift due to the Sun's rotational motion and is given per angular misalignment perpendicular to the rotational axis (1 arcsec is about 1 part in 1000 of r_s). The sensitivity of the Gaussian mode does not significantly decrease upon increasing its field of view from 0.5 to 1.1 solar radii, but a similarly sized flat-top beam should reduce the pointing sensitivity by 2 orders of magnitude compared to the current $0.5r_s$ setup.

On the other hand, with a larger aperture telescope, high spatial resolution could be achieved on the Sun. Indeed, sunlight from multiple positions in the solar disk could be coupled into individual single-mode fibers and spatially-resolved spectroscopy could be performed in parallel with a common local oscillator. Spatially and temporally resolved spectra could be used to probe the temporal evolution of granulation on the Sun, and to constrain the 3D magnetohydrodynamics code that simulate the solar photosphere. While the newly commissioned Daniel K. Inouye Solar Telescope (DKSIT) can also perform high resolution spectroscopic observations, frequency comb calibrated LHR could intrinsically provide frequency information with higher fidelity and precision.

An interesting direction for future work is to employ the frequency comb itself as the local oscillator in LHR. This could significantly broaden the instantaneous spectral bandwidth over which measurements could be made, by effectively channelizing the thermal light spectra around each comb tooth. For solar

physics, simultaneous coverage of several lines would allow exploration of a range of magnetic sensitivities and depths of formations in the solar photosphere. And for spectroscopy of the Earth's atmosphere, this would provide simultaneous information on multiple species (e.g. CH_4, CO_2, H_2O, ...), as well as full rovibrational spectra of molecular species, which is useful for temperature and pressure quantification. Preliminary experiments using frequency combs to directly measure thermal-like sources have been performed [27, 28]. However, in these works the thermal heterodyne signal required extremely long averaging times to emerge above the shot, thermal and electronic noise floors. A more fruitful direction may be to combine spectral demultiplexing with combs of high power per mode to optimize the SNR on an array of detectors. We provide a few scenarios in the Supplementary Material.

Focusing on the frequency content of a single line, the achievable frequency precision could be increased by discarding the line shape information. A signal proportional to the derivative of the spectral amplitude, suitable for use as an error signal to servo and lock the LO laser [44], can be generated by dithering the laser frequency and performing lock-in detection of the LHR output. Retrieval of such derivative signals have been previously demonstrated using LHR [45, 46], but not in the context of feeding back to and stabilizing the laser frequency. Locking the LO laser would make the average laser frequency a direct representation of a line's instantaneous center frequency, maximize the effective averaging time at the point of spectroscopic interest, and allow for continuous tracking of the line frequency against a laser frequency comb. Such measurements could complement helioseismic studies that also focus on single lines, such as the BISON and GONG networks [47, 48], by extending high precision radial velocity measurements to different wavelengths and atomic species.

Polarization of the thermal light is an aspect of our work that remains to be analyzed. As heterodyning is fundamentally a single-mode process, only light in the same polarization state as the LO will contribute to the signal. The absorption lines embedded in the solar spectrum are slightly polarized due to the Sun's magnetic field, and the Earth's atmosphere can in principle change the polarization of the detected light randomly at the few percent level [49]. While we have yet to see the direct effect of this noise source in our measurements, mitigation could either involve fully randomizing (scrambling) the polarization of the sunlight via agitation/rotation/squeezing of the SMF in which the solar light propagates, or splitting and then separately detecting the two orthogonal polarizations of the input solar light. The second approach would provide the full polarization information of the solar or atmospheric lines, which would be particularly beneficial for the analysis of Zeeman-sensitive lines.

Finally, the main results in this paper were demonstrated using the Sun as the thermal source, and a natural question to ask is whether LHR could be as interesting on other stars [50]. The largest obstacle to that is the antenna theorem [31], which places large constraints on the effective aperture and field of view. Alpha Centauri A for example, the nearest Sun-like star, would need to be viewed with a diffraction-limited aperture spanning about 30 m in order to get the same SNR as our results on the Sun, which only used a $\sim$1 mm diameter aperture. For unresolved objects, the maximum efficiency (η) of an LHR measurement scales with the filling factor of the source within the field of view (this derating can be simply estimated as the squared ratio of the angular radii of the star and of the collecting aperture's field of view). For cold or unresolved objects, LHR's signal-to-noise ratio takes a significant hit in comparison to the direct detection used in traditional spectrographs, which have an SNR similar in form to Eq. 2 but which instead scale with the square root of $\eta \langle n \rangle / (1 + \eta \langle n \rangle)$ [32]. That being said, we note that there are several telescopes presently planned or under construction (Giant Magellan Telescope, Thirty Meter Telescope, and Extremely Large Telescope) that would have apertures sufficient for LHR of nearby stars. While challenging, the introduction and continued improvement of photonic tools and optical frequency combs makes further study of LHR in the near- and mid-infrared a compelling cross-disciplinary field of exploration for precision spectroscopy and Doppler metrology in astronomy, atmospheric science, and remote sensing.

Funding. NIST (70NANB18H006) and NSF (AST-1310875, AST-1310885, AST-2009982, ATI 2009889, ATI 2009982)

Acknowledgments. The Center for Exoplanets and Habitable Worlds is supported by the Pennsylvania State University, the Eberly College of Science, and the Pennsylvania Space Grant Consortium. The authors further acknowledge helpful comments and discussions on the topic with Eugene Tsao, and Bill Swann. This work is a contribution of NIST and is not subject to copyright in the US. Mention of specific products or trade names is for technical and scientific information and does not constitute and endorsement by NIST.

Disclosures. The authors declare no conflicts of interest.

Data availability. Data underlying the results presented in this paper are not publicly available at this time but may be obtained from the authors upon reasonable request.

Supplemental document. See Supplement 1 for supporting content.

REFERENCES

1. K. Beloy, M. I. Bodine, T. Bothwell, S. M. Brewer, S. L. Bromley, J.-S. Chen, J.-D. Deschênes, S. A. Diddams, R. J. Fasano, T. M. Fortier, Y. S. Hassan, D. B. Hume, D. Kedar, C. J. Kennedy, I. Khader, A. Koepke, D. R. Leibrandt, H. Leopardi, A. D. Ludlow, W. F. McGrew, W. R. Milner, N. R. Newbury, D. Nicolodi, E. Oelker, T. E. Parker, J. M. Robinson, S. Romisch, S. A. Schäffer, J. A. Sherman, L. C. Sinclair, L. Sonderhouse, W. C. Swann, J. Yao, J. Ye, and X. Zhang, "Frequency ratio measurements at 18-digit accuracy using an optical clock network Boulder," Nature **591**, 564–569 (2021).
2. S. M. Brewer, J. . Chen, A. M. Hankin, E. R. Clements, C. W. Chou, D. J. Wineland, D. B. Hume, and D. R. Leibrandt, "$^{27}Al^+$ quantum-logic clock with systematic uncertainty below 10^{-18}," Phys. review letters **123** (2019).
3. S. A. Diddams, K. Vahala, and T. Udem, "Optical frequency combs: Coherently uniting the electromagnetic spectrum," Science **369**, eaay3676 (2020).
4. L.-S. Ma, Z. Bi, A. Bartels, K. Kim, L. Robertsson, M. Zucco, R. S. Windeler, G. Wilpers, C. Oates, L. Hollberg, and S. A. Diddams, "Frequency Uncertainty for Optically Referenced Femtosecond Laser Frequency Combs," IEEE J. Quantum Electron. **43** (2007).
5. L. A. M. Johnson, P. Gill, and H. S. Margolis, "Evaluating the performance of the NPL femtosecond frequency combs: agreement at the 10 -21 level," Metrologia **52**, 62–71 (2015).
6. Y. Yao, Y. Jiang, H. Yu, Z. Bi, and L. Ma, "Optical frequency divider with division uncertainty at the 10-21 level," Natl. Sci. Rev. **3**, 463–469 (2016).
7. A. T. Forrester, "Photoelectric Mixing as a Spectroscopic Tool," J. Opt. Soc. Am. **51**, 253 (1961).
8. W. T. Sullivan, *Classics in Radio Astronomy* (Springer Netherlands, Dordrecht, 1982).
9. B. Parvitte, V. Zéninari, C. Thiébeaux, A. Delahaigue, and D. Courtois, "Infrared laser heterodyne systems," Spectrochimica Acta - Part A: Mol. Biomol. Spectrosc. **60**, 1193–1213 (2004).

10. H. Nieuwenhuijzen, "An Optical Heterodyne Experiment on Stars," Mon. Notices Royal Astron. Soc. **150**, 325–335 (1970).
11. B. Peyton, A. DiNardo, S. Cohen, J. McElroy, and R. Coates, "An infrared heterodyne radiometer for high-resolution measurements of solar radiation and atmospheric transmission," IEEE J. Quantum Electron. **11** (1975).
12. T. Kostiuk and M. J. Mumma, "Remote sensing by IR heterodyne spectroscopy," Appl. Opt. **22**, 2644 (1983).
13. C. H. Townes, "Spatial interferometry in the mid-infrared region," J. Astrophys. Astron. **5**, 111–130 (1984).
14. R. T. Ku and D. L. Spears, "High-sensitivity infrared heterodyne radiometer using a tunable-diode-laser local oscillator," Opt. Lett. **1**, 84–86 (1977).
15. R. T. Menzies and R. K. Seals, "Ozone Monitoring with an Infrared Heterodyne Radiometer," Science **197**, 1275–1277 (1977).
16. G. Sonnabend, D. Wirtz, F. Schmülling, and R. Schieder, "Tuneable heterodyne infrared spectrometer for atmospheric and astronomical studies," Appl. Opt. **41**, 2978 (2002).
17. A. Rodin, A. Klimchuk, A. Nadezhdinskiy, D. Churbanov, and M. Spiridonov, "High resolution heterodyne spectroscopy of the atmospheric methane NIR absorption," Opt. Express **22**, 13825 (2014).
18. E. L. Wilson, M. L. McLinden, J. H. Miller, G. R. Allan, L. E. Ott, H. R. Melroy, and G. B. Clarke, "Miniaturized laser heterodyne radiometer for measurements of CO2 in the atmospheric column," Appl. Phys. B: Lasers Opt. **114**, 385–393 (2014).
19. J. Kurtz and S. O'Byrne, "Multiple receivers in a high-resolution near-infrared heterodyne spectrometer," Opt. Express **24** (2016).
20. J. Wang, C. Sun, G. Wang, M. Zou, T. Tan, K. Liu, W. Chen, and X. Gao, "A fibered near-infrared laser heterodyne radiometer for simultaneous remote sensing of atmospheric CO2 and CH4," Opt. Lasers Eng. **129** (2020).
21. A. D. Sappey and B. P. Masterson, "Development of a passive optical heterodyne radiometer for near and mid-infrared spectroscopy," Appl. Opt. **60**, 884–893 (2021).
22. L. Delbouille, G. Roland, J. Brault, L. Testerman, K. P. N. Observatory, and U. de Liège. Institut d'astrophysique, "Photometric atlas of the solar spectrum from 1,850 to 10,000 cm-1," Tech. rep., Kitt Peak National Observatory (1981).
23. Solar FTS spectrum provided by the BASS2000 website, http://bass2000.obspm.fr/solar_spect.php.
24. X. Dumusque, A. Glenday, D. F. Phillips, N. Buchschacher, A. C. Cameron, M. Cecconi, D. Charbonneau, R. Cosentino, A. Ghedina, D. W. Latham, C.-H. Li, M. Lodi, C. Lovis, E. Molinari, F. Pepe, S. Udry, D. Sasselov, A. Szentgyorgyi, and R. Walsworth, "HARPS-N OBSERVES THE SUN AS A STAR," The Astrophys. J. **814**, L21 (2015).
25. H. M. Cegla, C. A. Watson, S. Shelyag, M. Mathioudakis, and S. Moutari, "Stellar surface magnetoconvection as a source of astrophysical noise. iii. sun-as-a-star simulations and optimal noise diagnostics," The Astrophys. journal **879**, 55 (2019).
26. J. Crass, B. S. Gaudi, S. Leifer, C. Beichman, C. Bender, G. Blackwood, J. A. Burt, J. L. Callas, H. M. Cegla, S. A. Diddams *et al.*, "Extreme precision radial velocity working group final report," arXiv preprint arXiv:2107.14291 (2021).
27. F. R. Giorgetta, I. Coddington, E. Baumann, W. C. Swann, and N. R. Newbury, "Dual Frequency Comb Sampling of a Quasi-Thermal Incoherent Light Source," in *Conference on Lasers and Electro-Optics 2010,* (OSA, Washington, D.C., 2010).
28. S. Boudreau and J. Genest, "Referenced passive spectroscopy using dual frequency combs," Opt. Express **20** (2012).
29. D. D. S. Hale, M. Bester, W. C. Danchi, W. Fitelson, S. Hoss, E. A. Lipman, J. D. Monnier, P. G. Tuthill, and C. H. Townes, "The Berkeley Infrared Spatial Interferometer: A Heterodyne Stellar Interferometer for the Mid-Infrared," The Astrophys. J. **537**, 998–1012 (2000).
30. V. V. Protopopov, *Laser heterodyning*, vol. 149. (Springer, Heidelberg;New York;, 2009;2014;).
31. A. E. Siegman, "The Antenna Properties of Optical Heterodyne Receivers," Appl. Opt. **5**, 1588 (1966).
32. J. Zmuidzinas, "Thermal noise and correlations in photon detection," Appl. Opt. **42**, 4989 (2003).
33. S. L. Gilbert, W. C. Swann, and C.-M. Wang, "Hydrogen cyanide h13c14n absorption reference for 1530 nm to 1565 nm wavelength calibration–srm 2519a," NIST Special Publ. **260**, 137 (2005).
34. W. C. Swann and S. L. Gilbert, "Line centers, pressure shift, and pressure broadening of 1530-1560 nm hydrogen cyanide wavelength calibration lines," J. Opt. Soc. Am. B **22**, 1749–1756 (2005).
35. J. Jennings, S. Halverson, R. Terrien, S. Mahadevan, G. Ycas, and S. A. Diddams, "Frequency stability characterization of a broadband fiber Fabry-Pérot interferometer," Opt. Express **25** (2017).
36. A. Kramida, Yu. Ralchenko, J. Reader, and and NIST ASD Team, NIST Atomic Spectra Database (ver. 5.8), [Online]. Available: `https://physics.nist.gov/asd` [2021, June 19]. National Institute of Standards and Technology, Gaithersburg, MD. (2020).
37. G. Nave, S. Johansson, R. Learner, A. Thorne, and J. Brault, "A new multiplet table for fe i," The Astrophys. J. Suppl. Ser. **94**, 221–459 (1994).
38. A. Prša, P. Harmanec, G. Torres, E. Mamajek, M. Asplund, N. Capitaine, J. Christensen-Dalsgaard, É. Depagne, M. Haberreiter, S. Hekker, J. Hilton, G. Kopp, V. Kostov, D. W. Kurtz, J. Laskar, B. D. Mason, E. F. Milone, M. Montgomery, M. Richards, W. Schmutz, J. Schou, and S. G. Stewart, "NOMINAL VALUES FOR SELECTED SOLAR AND PLANETARY QUANTITIES: IAU 2015 RESOLUTION b3," The Astron. J. **152**, 41 (2016).
39. A. K. Pierce, C. D. Slaughter, and D. Weinberger, "Solar limb darkening in the interval 7404-24 018 , ii," Sol. physics **52**, 179–189 (1977).
40. S. Kanodia and J. Wright, "Python leap second management and implementation of precise barycentric correction (barycorrpy)," Res. Notes AAS **2**, 4 (2018).
41. J. T. Wright and S. Kanodia, "Barycentric corrections for precise radial velocity measurements of sunlight," The Planet. Sci. J. **1**, 38 (2020).
42. G. Stefansson, S. Mahadevan, L. Hebb, J. Wisniewski, J. Huehnerhoff, B. Morris, S. Halverson, M. Zhao, J. Wright, J. O'rourke, H. Knutson, S. Hawley, S. Kanodia, Y. Li, L. M. Z. Hagen, L. J. Liu, T. Beatty, C. Bender, P. Robertson, J. Dembicky, C. Gray, W. Ketzeback, R. McMillan, and T. Rudyk, "Toward space-like photometric precision from the ground with beam-shaping diffusers," The Astrophys. J. **848**, 9 (2017).
43. I. Ermolli, K. Shibasaki, A. Tlatov, and L. van Driel-Gesztelyi, "Solar cycle indices from the photosphere to the corona: Measurements and underlying physics," Space science reviews **186**, 105–135 (2014;2017;).
44. M. Weel and A. Kumarakrishnan, "Laser-frequency stabilization using a lock-in amplifier," Can. J. Phys. **80**, 1449–1458 (2002).
45. P. Martín-Mateos, O. E. Bonilla-Manrique, and C. Gutiérrez-Escobero, "Wavelength modulation laser heterodyne radiometry," Opt. Lett. **43**, 3009–3012 (2018).
46. P. Martín-Mateos, A. Genner, H. Moser, and B. Lendl, "Implementation and characterization of a thermal infrared laser heterodyne radiometer based on a wavelength modulated local oscillator laser," Opt. Express **27**, 15575–15584 (2019).
47. W. J. Chaplin, Y. Elsworh, R. Howe, G. R. Isaak, C. P. McLeod, B. A. Miller, H. B. Van Der Raay, S. J. Wheeler, and R. New, "Bison performance," Sol. physics **168**, 1–18 (1996).
48. J. W. Harvey, F. Hill, R. P. Hubbard, J. R. Kennedy, J. W. Leibacher, J. A. Pintar, P. A. Gilman, R. W. Noyes, A. M. Title, J. Toomre, R. K. Ulrich, A. Bhatnagar, J. A. Kennewell, W. Marquette, J. Patrón, O. Saá, and E. Yasukawa, "The global oscillation network group (gong) project," Science **272**, 1284–1286 (1996).
49. G. N. Plass and G. W. Kattawar, "Polarization of the radiation reflected and transmitted by the earth's atmosphere," Appl. Opt. **9**, 1122–1130 (1970).
50. A. D. Sappey, P. Masterson, and B. A. Sappey, "Passive optical heterodyne spectroscopy measurement of the doppler shift of fe(i) lines induced by the rotational velocity of the sun," J. Opt. Soc. Am. B **37**, 3829–3840 (2020).